WARWICK
THE UNIVERSITY OF WARWICK

Original citation:
Parker, Alexander S., Al Botros, Rehab, Kinnear, Sophie L., Snowden, Michael E., McKelvey, Kim M. (Kim Martin), Ashcroft, Alexander T., Carvell, Mel, Joiner, Andrew, Peruffo, Massimo, Philpotts, Carol and Unwin, Patrick R.. (2016) Combinatorial localized dissolution analysis : application to acid-induced dissolution of dental enamel and the effect of surface treatments. Journal of Colloid and Interface Science, 476. pp. 94-102.

Permanent WRAP URL:
http://wrap.warwick.ac.uk/81648

warwick.ac.uk/lib-publications

Combinatorial Localized Dissolution Analysis: Application to Acid-induced Dissolution of Dental Enamel and the Effect of Surface Treatments

Alexander S. Parker,[†a] Rehab Al Botros,[†a] Sophie L. Kinnear,[a] Michael E. Snowden,[a] Kim McKelvey,[a] Alexander T. Ashcroft,[b] Mel Carvell,[b] Andrew Joiner,[b] Massimo Peruffo,[c] Carol Philpotts,[c] and Patrick R. Unwin[a*]

a Electrochemistry and Interfaces Group, Department of Chemistry, University of Warwick, Coventry CV4 7AL.
b Unilever Oral Care, Quarry Road East, Bebington, Wirral CH63 3JW, UK.
* Corresponding author: Patrick R. Unwin, Electrochemistry and Interfaces Group, Department of Chemistry, University of Warwick, Coventry CV4 7AL, UK.
† These authors contributed equally to this work

A combination of scanning electrochemical cell microscopy (SECCM) and atomic force microscopy (AFM) is used to quantitatively study the acid-induced dissolution of dental enamel. A micron-scale liquid meniscus formed at the end of a dual barrelled pipette, which constitutes the SECCM probe, is brought into contact with the enamel surface for a defined period. Dissolution occurs at the interface of the meniscus and the enamel surface, under conditions of well-defined mass transport, creating etch pits that are then analysed via AFM. This technique is applied to bovine dental enamel, and the effect of various treatments of the enamel surface on acid dissolution (1mM HNO_3) is studied. The treatments investigated are zinc ions, fluoride ions and the two combined. A finite element method (FEM) simulation of SECCM mass transport and interfacial reactivity, allows the intrinsic rate constant for acid-induced dissolution to be quantitatively determined. The dissolution of enamel, in terms of Ca^{2+} flux ($j_{Ca^{2+}}$), is first order with respect to the interfacial proton concentration and given by the following rate law: $j_{Ca^{2+}} = k_0 [H^+]$, with k_0= 0.099 ±0.008 cm.s^{-1}. Treating the enamel with either fluoride or zinc slows the dissolution rate, although in this model system the partly protective barrier only extends around 10-20 nm into the enamel surface, so that after a period of a few seconds dissolution of modified surfaces tends towards that of native enamel. A combination of both treatments exhibits the greatest protection to the enamel surface, but the effect is again transient.

Introduction

The dissolution of solid materials is an area of significant interest[1] across many fields, including the earth sciences,[2, 3] corrosion science,[4] and the life sciences, [5] as well as in chemistry.[6-12] Studies of the mechanism and kinetics of dissolution processes are important for both fundamental understanding and for various technical applications. This area requires methodologies that can probe dissolution under conditions of high and well-defined mass transport,[13] so that surface kinetics can be extracted free from convolution from mass transport.[13, 14] This means that dissolution experiments must deliver sufficiently high and well-defined mass transport rates that surface kinetics are manifest in the measurement.

This paper describes a powerful combinatorial approach for dissolution studies, in which a large number of micron scale measurements are made rapidly on a small area of a single sample surface, for which different portions have been treated in different ways. The focus is on the acid-induced dissolution of dental enamel as an exemplar system, and one which is also of significant interest. Enamel is the hardest mineral found in the human body,[15] forming the outer protective layer of teeth. Its main component is calcium hydroxyapatite (HAP, $Ca_{10}(PO_4)_6(OH)_2$) which makes up more than 95% of enamel by weight,[16] with the remainder comprised of a matrix of organic molecules, macromolecules and water.[17] Dental enamel is constructed from rods or prisms, each containing a tightly packed mass of HAP nanocrystallites in a highly orientated and organised structure.[18] Once formed, enamel has no vascular or nerve system, and can only regenerate minerals through remineralisation processes in the oral cavity.[19] Conversely, the enamel layer can be affected adversely through acid-induced dissolution processes associated with dental caries or erosion from the modern diet.[20-22]

Acid attack of HAP is reasonably described by the following reaction:[23]

$$Ca_{10}(PO_4)_6(OH)_{2\ (S)} + 8H^+_{(aq)} \rightleftharpoons 10\ Ca^{2+}_{(aq)} + 6HPO_4^{2-}_{(aq)} + 2\ H_2O\ (1)$$
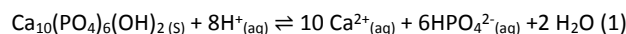
This is the primary process of tooth demineralization: protons react with HAP, which releases Ca^{2+} and HPO_4^{2-} ions into the solution,[15, 24, 25] coupled with further solution processes (*vide infra).*

As highlighted above, to understand the relative contribution of surface processes and mass transport to demineralisation rates, experiments need to be carried out under controlled, calculable, and sufficiently high mass transport conditions.[13, 14, 23, 26] The

1

main approach, with well-defined mass transport, used in studies of enamel and HAP dissolution is the rotating disk (RD) method.[27-33] However, while RD method it is often restricted to bulk solution measurements which places severe limitations on the time and spatial resolution of the technique.[13] This is particularly detrimental for the investigation of surface treatments that have a transient (temporary) effect, which may be short lived. To elucidate such effects requires methods with high time resolution. In terms of spatial resolution, a number of studies have used high resolution microscopy to study enamel dissolution at the nanoscale[20, 34-41] However, with the exception of scanning electrochemical microscopy,[40] the approaches often have rather low mass transport rates and all require the sample to be exposed to solution for long periods, making it difficult to monitor transient effects on dissolution, such as the influence of surface treatments.

Several treatments have been used to protect enamel from acid dissolution.[42, 43] It is well documented that treatment of enamel with fluoride results in a surface layer of fluoridated hydroxyapatite and fluorapatite[44-47] which resists acid attack better than natural enamel,[48, 49] thus inhibiting demineralization.[48, 50] The effect of Zn^{2+} treatment of enamel also decreases the loss of Ca^{2+} and PO_4^{3-} ions from the surface. The binding of Zn^{2+} is proposed to lead to the precipitation of an apatite-like phase, and the formation of a zinc complex at the surface of enamel has been suggested.[47, 51-54]

The work presented here employs a new approach for the study of dissolution processes, coupling localized measurements with high and controlled mass transport through the use of SECCM. [55-59] The aim is to demonstrate the methodology and to gain a better understanding of the acid induced dissolution process on enamel surfaces as well as the effect of treating the enamel surface with zinc and fluoride. Localized dissolution is achieved by confining the experiment to the meniscus of a pipette with a diameter ca.1 μm, and making a series of such measurements, with different exposure times, across the surface. Migration of ions in the probe geometry allows fast surface kinetics can be investigated.[56] In essence SECCM is used as a tool to allow very fine control of the delivery of acid to the enamel surfaces resulting in localized etch pits. These dissolution etch pits are then analysed using AFM and, using a finite element method (FEM) simulation, the intrinsic rate for proton induced dissolution (Ca^{2+} release) is extracted. We have presented preliminary data using this method as part of a multi technique approach to elucidate a new treatment for enamel erosion that was presented in a special issue.[60] Here, we apply the technique in much more detail to common treatments of dental enamel, highlighting the spatial resolution of the approach and developing a full theoretical model to quantitatively analyse data.

Experimental details

Solutions

All solutions were prepared using resistivity 18.2 MΩ cm (25°C) water (Purite). Etching solutions (50 mM KNO_3 and 1 mM HNO_3 (Sigma-Aldrich)) were prepared daily (pH 3.3, Denver Instruments UB-10 pH meter). Zinc salt solutions used for enamel pretreatment were made using 1000 ppm of Zn^{2+} from $ZnCl_2$ (Sigma-Aldrich). Fluoride solutions for enamel pretreatment were 1000 ppm of F^- using NaF (Sigma-Aldrich).

Sample preparation

Bovine enamel samples were received from Unilever as 36 mm^2 area blocks polished to a 3 μm root mean squared (rms) roughness, as measured by AFM (Bruker). The samples were then further polished using diamond lapping particles on a silk polishing pad, starting with 3 μm sized particles and slowly working down to 50 nm (Buehler). The polishing was carried out until a mirror finish was achieved with an rms of 1.5 ± 0.6 nm measured by AFM. Three different treatments were applied to each enamel block, one treatment per section, with rinsing of the sample in Purite water between treatments. To selectively treat a particular section, a low tack polyester tape (3M) was used to protect all but the area of interest, before submerging the sample in the treatment solution for 2 minutes (see Fig 1). The treatments used were 1000 ppm F^-, 1000 ppm Zn^{2+}, and a sector of the enamel was also subjected to a combined treatment with F^- and Zn^{2+}, applied sequentially as depicted in Fig 1.
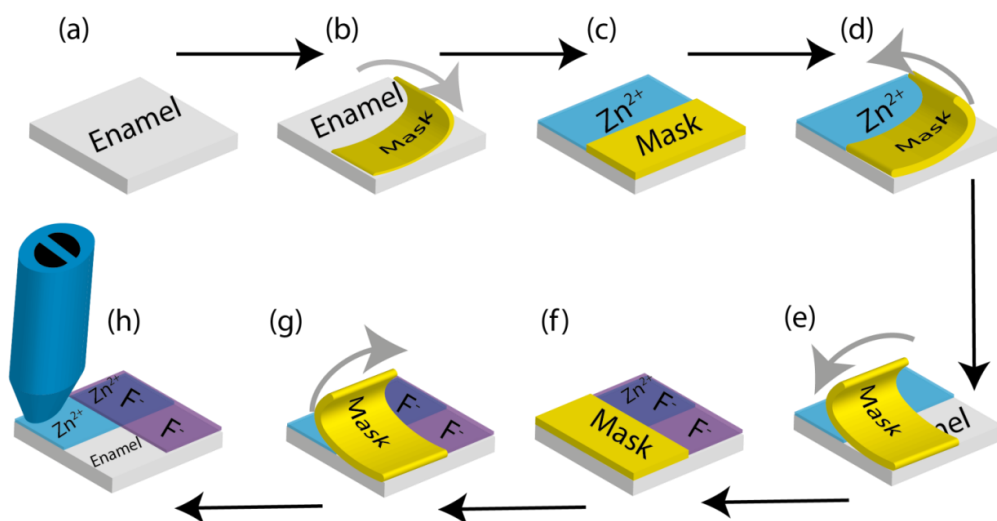
Fig 1: Representation of the localized treatments applied to an enamel block: a) Enamel block polished before any treatment applied; b) Half the sample masked off with polyester tape; c) Zn^{2+} treatment applied to sample; d) Polyester mask removed; e) Mask reapplied at 90° rotation; f) Zn^{2+} treatment applied to sample; g) Mask removed; h) the final surface studied by SECCM.

SECCM method

The SECCM tips used were fabricated from 1.5 mm diameter borosilicate theta capillaries (Harvard Apparatus) that were pulled to a sharp point using a P-2000 laser puller (Sutter Instruments Co.). After pulling, the tip of the resulting pipette was oval and approximately 800 nm across the main axis. A representative tip is pictured in Fig 2(a). Each pipette was filled with the etching solution and a quasi-reference counter electrode (QRCE) comprising an AgCl-coated Ag wire was inserted into each barrel.

The SECCM technique was set up as recently described.[59] The pipette was positioned close to the enamel surface using a manual micrometer system (M-461 series, Newport) aided by a digital camera (Pixelink). Fine positioning of the pipette was achieved using a piezoelectric positioner system with a range of 38 µm normal to the substrate, in the *z*-axis (P-753.3CD positioner, Physik Instrumente) and 300 µm parallel to the substrate in the *x*- and *y*-axes (Nano-Bio300, Mad City Labs). A potential of 0.25 V was applied between the QRCEs in the barrels of the theta pipette using a home-built instrument controlled via LabVIEW 2011 and a field programmable gate array card (PCI-783R, National Instruments). An oscillation of 80 nm amplitude was applied to the *z*-position of the tip, with a frequency of 233.5 Hz, using an external lock-in amplifier (SR830DSP, Stanford Research Systems), and the resulting alternating current (AC) magnitude at the driving frequency was measured and used to inform on the meniscus condition. An approach-hold-withdraw method, as illustrated in Fig 2(b), was used to carry out local dissolution at the enamel surface with different solution contact times. First, as shown in Fig 2(b)(i), the *z*-piezo was used to move the pipette towards the surface and the approach was stopped when the meniscus made contact with the surface (without the pipette itself making contact) as evidenced by a sudden change in the AC value. Typically, a threshold value of one order of magnitude higher than the background AC measured when the tip was in air.[61] The meniscus was held in contact with the surface for a precise period of time (Fig 2(b)(ii)), after which the pipette was rapidly translated away from the surface (20 µm s^{-1}), breaking meniscus contact (Fig 2(b)(iii)). The pipette was then moved laterally to the next approach location at a velocity of 1 µm s^{-1} (taking 5 seconds), in this time the solution in the meniscus retuned to its initial conditions (equilibrium reached in << 1 sec).[59] This procedure was used to prepare an array of local etch features, following the pattern described in Fig 2(c), which also shows the path of the pipette. The array created in this experiment started with a 1 s meniscus hold time on the surface, and this was increased by 1 s for each subsequent position, up to a total of 16 s. Six arrays were created in each treatment section of an enamel surface and a total of four bovine enamel samples were studied, meaning that 24 separate arrays were created for the four different surfaces. Optical images showing an experiment in progress and an example of the resultant pit arrays are provided in Fig 3.
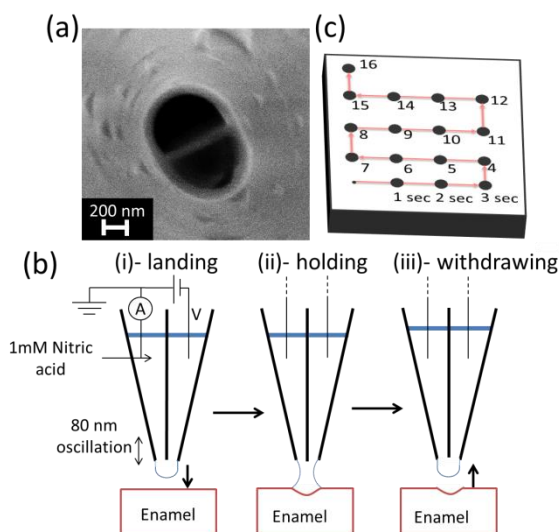
3

Fig 2: (a) SEM image of a pipette tip. (b) Representation of the experimental setup used. The approach-hold-withdraw cycle and probe path used in SECCM experiments. (i) Probe approaches enamel surface. (ii) Meniscus makes contact with the surface and is held for a set time. (ii) The probe is withdrawn and meniscus removed from the surface. (c) The path the probe takes during the whole array used. Red line represents tip path. Meniscus contact in each spot is 1 second longer than the previous spot.
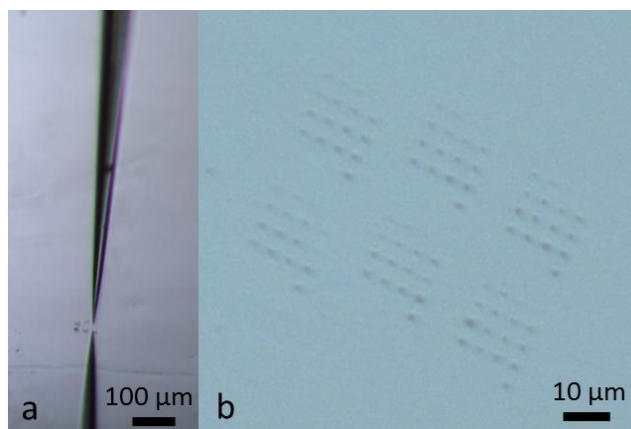

Fig 3: Optical images of: a) an experiment in progress; b) close up image of arrays of dissolution pits formed on a surface.

Atomic Force Microscopy

The SECCM etch pits were characterized using a Bruker Nano Enviroscope AFM with a Nanoscope IV controller in tapping mode. Tips used were 0.01-0.025 Ω-cm Sb doped Si cantilevers (Veeco). The resultant images were analysed using SPIP 6.0.10 software.

Theory and Simulations

A 3D finite element method (FEM) model was used to extract the acid induced dissolution rate of enamel. The theta pipette presents a symmetry plane perpendicular to the pipette septum such that it was possible to model only half a pipette, for computational efficiency, as illustrated in Figure 4. Values for the parameters used to describe the theta pipette geometry were typical values obtained from SEM images of the pipette: the major pipette radius perpendicular to the septum (*mpr* = 440 nm); the minor pipette tip radius parallel to the septum (*mptr* = 260 nm); septum width (*tw* = 74 nm), pipette semi-angle (*semi-ang* = 2.4°).

4

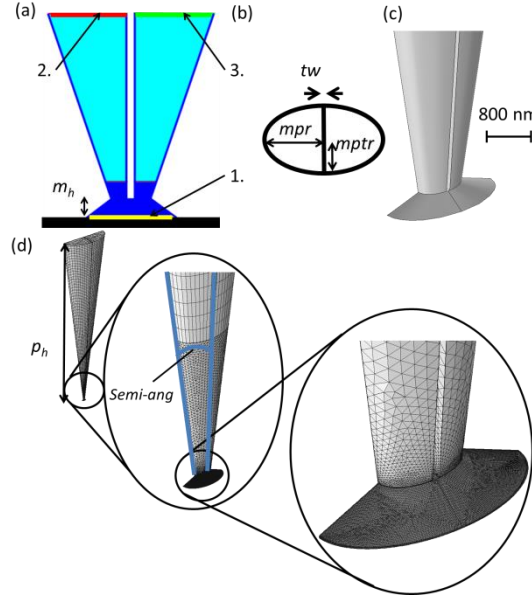| species	diffusion coefficient (D) (cm^2 s^{-1})	Charge (z)
Ca^{2+}	0.792x10^{-5}	2
HPO$_4^{2-}$	0.759x10^{-5}	-2
H$_2$PO$_4^-$	0.959 x10^{-5}	-1
H$_3$PO$_4$	0.882 x10^{-5}	0
H$^+$	9.311 x10^{-5}	1

Fig 4: The pipette geometry used. (a) 2D representation of the 3D simulations. (b) 2D representation of the end of the pipette. (c) The simulation geometry used zoomed into the region of the meniscus. (d) 3D representation of pipette also showing the meshing points used in experiments.
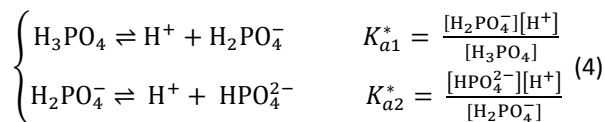
For simplicity the simulation assumed a planar enamel surface due to the relatively shallow pits formed after etching, especially at the short times. However, the meniscus contact width (m_w) that is shown in Figure 4(a) was adjusted for each experimental time simulated, as informed from AFM data of etch pits. The meniscus height (m_h = 300 nm), and the fraction of the potential that falls across the simulation boundaries (E_f) were determined by matching the ionic conductance current in the simulation (with an inert substrate surface) to the experimental barrel current of an approach to an inert silicon oxide wafer substrate.[56] The pipette height (p_h = 100 µm), which is the height of the tip domain that was simulated, was chosen to be sufficiently large so not to influence the results of the simulation.[59] All simulations were carried out using the FEM simulation software Comsol Multiphysics (v4.3, Comsol AB) with LiveLink for Matlab (R2011a, Mathworks).

The Nernst-Planck equation (eq. 2) coupled with the electroneutrality condition (eq. 3) was solved to determine ionic concentration distributions in the pipette and meniscus domains:

$$\nabla \cdot (-D_i \nabla c_i - z_i u_i F c_i \nabla V) = R_i \qquad (2)$$

$$\sum_i z_i c_i = 0. \qquad (3)$$

where c_i is concentration, D_i is diffusion coefficient,[56] z_i is charge, u_i is ionic mobility (calculated based on the Einstein equation) of species i, F is the Faraday constant, and V is the electric field (between the 2 QRCEs). The values used are given in Table 1. R_i indicates reactions leading to the formation or loss of species i within the field. Species in the solution were always kept at equilibrium, described by the following equations.

$$\begin{cases} H_3PO_4 \rightleftharpoons H^+ + H_2PO_4^- & K_{a1}^* = \frac{[H_2PO_4^-][H^+]}{[H_3PO_4]} \\ H_2PO_4^- \rightleftharpoons H^+ + HPO_4^{2-} & K_{a2}^* = \frac{[HPO_4^{2-}][H^+]}{[H_2PO_4^-]} \end{cases} \quad (4)$$

where K_{1a}^* and K_{2a}^* are acid dissociation constants for H_3PO_4 and $H_2PO_4^-$, respectively, corrected for the ion activity coefficients using MINEQL⁺ (Chemical Equilibrium Modelling System v4.6). In this simulation, convection from the electroosmotic flow was reasonably assumed to be negligible and so was not included because diffusion and migration play a much larger role under the experimental conditions.[58] As the experimental contact times (1-16 s) were much longer than the time needed to reach steady-state in the pipette, it was reasonable to assume steady-state dissolution for the simulation.[56]

The initial concentrations for Ca^{2+}, HPO_4^{2-}, $H_2PO_4^-$, and H_3PO_4 were assigned to zero in the simulated domain. The bulk concentrations, (i) were maintained at boundaries 2 and 3 (Figure 4(a)) with the following equation:

$$c_i = c_i * \qquad\qquad (5)$$

is initial concentration of species i. To simulate the bias, $0\ V$ was applied to surface 3 (one barrel), and E_f was applied to surface 2 (the other barrel).[56]

At the interface between the meniscus and the enamel surface, represented in 2D (Figure 4(a)) with surface 1 as enamel (yellow), a flux relation was applied to represent the dissolution process:

$$
\begin{cases}
-n.\,N_{Ca^{2+}} & = & k_0.[H^+].\left(\dfrac{10}{8}\right) \\[2mm]
-n.\,N_{H_2PO_4^{2-}} & = & k_0.[H^+].\left(\dfrac{6}{8}\right) \\[2mm]
-n.\,N_{H^+} & = & -\,k_0.[H^+]
\end{cases}
$$

$$(6)$$

where n is the inward unit vector and N_i is flux vector of species i, The intrinsic rate constant for dissolution is K_0.

The fractions $\left(\dfrac{10}{8}\right)$ and $\left(\dfrac{6}{8}\right)$ represents the stoichiometry coefficients of the acid dissolution reaction (eq. 1). All other boundaries, pipette walls and meniscus sides, were considered to be electrically insulating and have no flux (normal).

Results and Discussion

Etch Pit analysis

Six arrays (each comprising 16 etch pits) were generated on each of the four enamel samples for each treatment. This resulted in 384 etch pits for each of the four treatment conditions, all of which were analysed using AFM. A representative AFM image of an array is shown in Fig 5. There is a noticeable trend towards deeper and wider dissolution pits with increased time. It can also be seen that SECCM dissolution results in highly localised dissolution at the position of meniscus contact with the enamel surface. The volume of the pits for each hold time was averaged across all the arrays and samples to produce Fig 6(a), which shows pit volume against meniscus contact time for untreated enamel, F⁻ treated enamel, Zn^{2+} treated enamel and the combined treatment. These data highlight that the etch pit volume increases with time for all surface types, but the extent of dissolution is greatest for untreated enamel. Treatment of the surfaces inhibits the extent of dissolution, although the difference from the untreated samples was most noticeable at short times. This trend is also evident in the plot of pit depth vs. time (Fig 6(b)), with the treated surfaces showing much smaller pit depths overall, and for all surfaces the pit depth increasing with time.
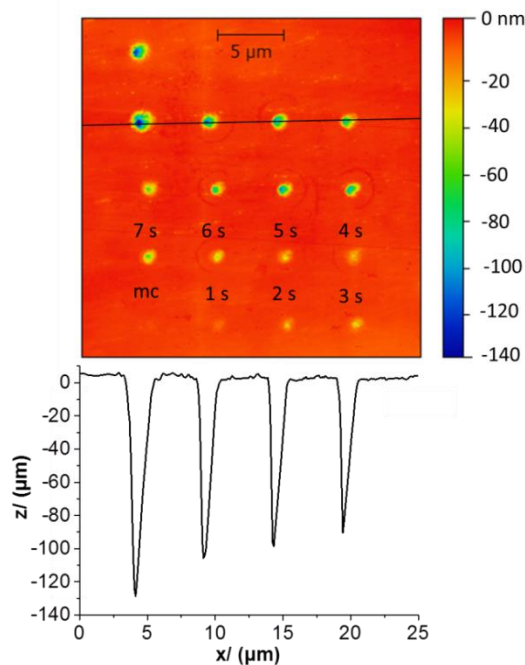
Fig 5: Typical array of etch pits formed using SECCM. Black line marks point of the profile at the bottom of the AFM image. The first point only makes momentary contact (mc), used for orientation of the sample.

In order to elucidate quantitative dissolution rates, it was necessary to know the pit diameter (Fig 6(c)), which relates to the area of meniscus contact. The change in diameter, and thus the area of contact between the meniscus and the surface, was taken into account and inputted into the simulations used to analyse the data i.e. a time dependent meniscus area was considered to ensure that surface fluxes were determined with high accuracy (*vide infra,* e.g. Figure 8).

Overall, the treatments appear to show F^- treatment providing more protection of the enamel surface to acid attack than Zn^{2+} treatment, with the combined treatment providing the greatest protection. However, at longer times, the treatments are less effective, based on the data in Figure 6. This is because the treatments only effect the surface layer of the enamel. The treatment does not penetrate substantially into the sample and protect the subsurface; this indicates these surface treatments are suitable if applied regularly.
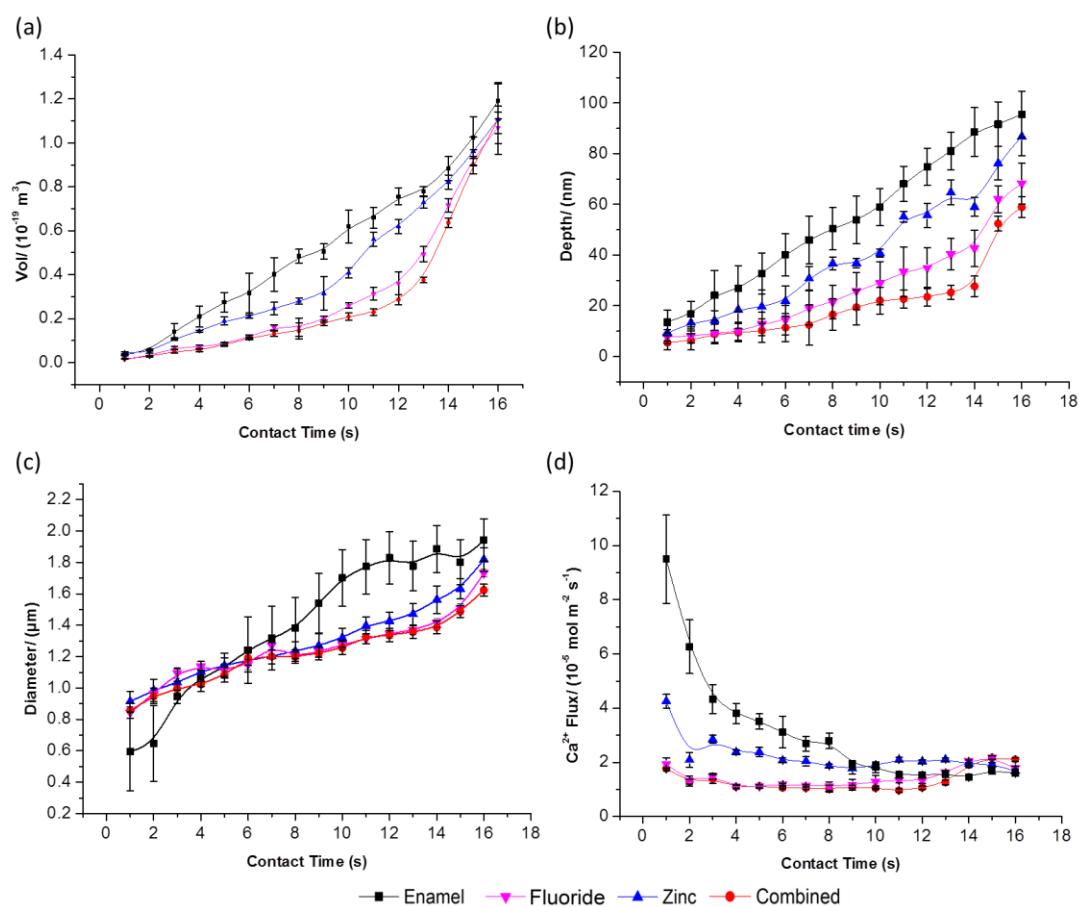
Fig 6: Plots of: (a) average etch pit volume, (b) average pit depth, (c) average pit diameter, (d) average Ca^{2+} flux as a function of time. Error bars show standard error of the mean, n=24. Curves through the points are to guide the eye.

The flux of Ca^{2+} (mol cm^{-2} s^{-1}) was determined using the time-dependent pit volume and area (calculated using SPIP 6.0.10 software) to calculate the molar amount of enamel removed (density of enamel is 3.16 g cm^{-3}, molar mass is 502 g mol^{-1}).[15-19, 63] The average flux for each contact time for the different enamel substrates is shown in Fig 6(d).

Table 2: Calculated intrinsic rate constants for the different enamel substrates. Error is standard error of the mean (n=384).

Sample	Intrinsic rate constant (k_0) for Ca^{2+} release (cm s^{-1})
Enamel	0.099 ±0.008
Zinc treated	0.058 ±0.007
Fluoride treated	0.033 ±0.008
Combined treated	0.025 ±0.005

All values are statistically different (p < 0.01) analysed by ANOVA and Tukey-Kramer analysis.

Simulations

The model described earlier was implemented to calculate Ca^{2+} fluxes as a function of k_0 which was varied in the simulations between 1×10^{-3} cm s^{-1} and 7×10^{-5} cm s^{-1}. The ratio of the diameter of contact area (obtained from AFM images of the pits, as described) to the diameter of the pipette was varied between 0.5 and 3. Fig 7 shows example concentration profiles for the key species involved in the acid attack and dissolution process for a rate constant, k_0=0.08 cm s^{-1}, which is at the upper end of those

measured experimentally (*vide infra*). It can be seen that protons are significantly consumed at the enamel surface (interfacial concentration *ca.* 0.1 mM) but that, even with this rate constant, there is some contribution from surface kinetics, which can be determined. The profiles also show that there is some asymmetry in the transport of ions to and from the surface due to the electric field between the 2 QRCEs in the pipette.[56]
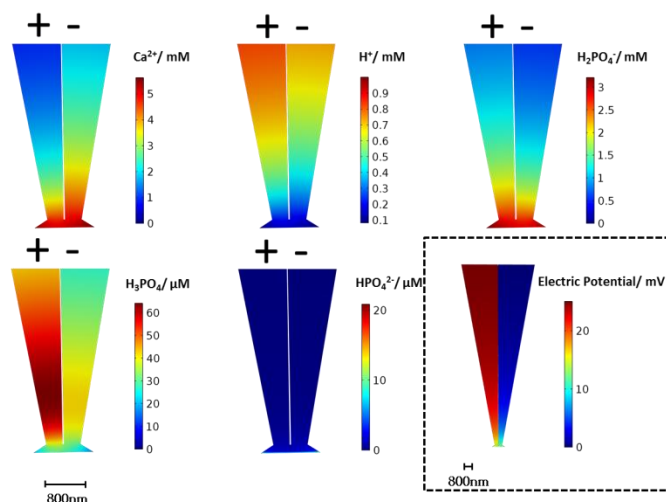

Fig 7: The concentration profiles of simulated species and electric potential at the end of the tip using an intrinsic rate constant, k_0, of 0.08 cm s^{-1}.

Determination of dissolution kinetics

A 3-D working plot showing the interfacial calcium ion flux from the enamel surface as a function of the dissolution (acid attack) rate constant and ratio of meniscus radius to pipette radius ratio is shown in Figure 8. The experimental data yield $j_{Ca^{2+}}$, as described above, along with the area of meniscus contact, leaving the kinetic term, k_0, which can then easily be determined. This calibration surface was used to derive the rate constant using the experimental results for all four treatment conditions and over all times. The average rate constant for each treatment is shown in Table 2. The result for the untreated enamel substrate is comparable to that of our previous work, (0.1 ±0.05 cm s^{-1}) using a different local method giving great confidence in the technique.[30] In particular, it proves that there are no deleterious issues, for example, from solution that could have been left behind from meniscus contact. As described above, it can be seen that F$^-$ treatment is more effective than Zn^{2+}, and that the two combined gives the best barrier to acid attack of enamel. This is important new information for the protection of enamel against acid attack. The variation between the rates constants for different treatments was proven to have statistical significance by using one-way analysis of variance (ANOVA) (p = 2.9x10^{-9}, 99%).

Conclusions

This study has presented a new method of combinatorial localized dissolution analysis highlighting the ability of SECCM to make multiple, rapid, localized, and independent measurements on a surface, under conditions of highly defined and fast mass transport. Combined with AFM analysis of the resulting etched features, this provides a powerful platform to investigate surface processes. In the present study, by following the dissolution reaction with time, it has been possible to elucidate the efficacy of surface treatments on enamel dissolution, and how this changes during etching. With the additional information provided by FEM modelling, quantitative kinetic information about the surface reaction has been extracted.
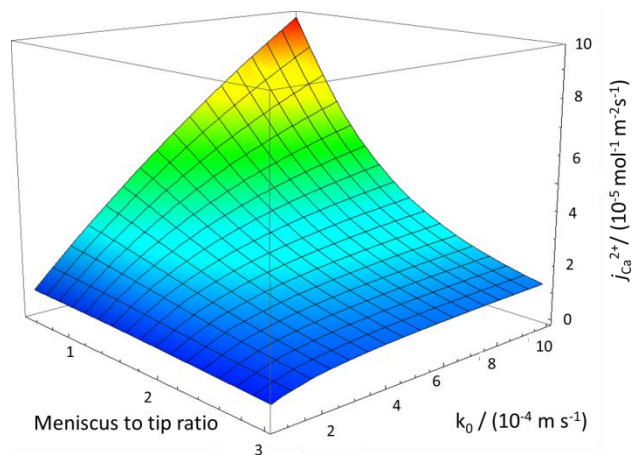
Fig 8: Simulated results showing Ca^{2+} flux (mol m^{-2} s^{-1}) vs. intrinsic rate constant of dissolution (m s^{-1}) vs. meniscus to tip ratio.

This method has proven to be particularly powerful for the investigation of dental enamel surfaces, which may show some inter-sample variability. With this approach herein, a single sample can be subjected to multiple treatments in different locations and their relative efficacy assessed, removing inter-sample effects. A particularly powerful aspect of the technique is that dissolution can be monitored for very short times, which is very beneficial as surface treatments often provide only a thin, transient coating, as shown herein. We expect that this approach could have myriad applications in the future for examining surface coatings and treatments. Although not exploited in this study, it should also be pointed out that dissolution can be monitored via the ion-conductance current during meniscus contact[59] which further enhances the capabilities of this technique.

For the systems studied, it has been found that both zinc and fluoride act initially to protect enamel from acid-induced dissolution, with fluoride having the greatest effect, whilst a combination of both treatments provided the optimum protection. This study demonstrates that the method outlined can be used to test treatments in a high throughput, automated approach to test single and multiple (combination) treatments of a surface quickly and effectively.

Acknowledgements

Notes and references

Corresponding Author

* To whom correspondence should be addressed E-mail: p.r.unwin@warwick.ac.uk.

Author Contributions

All authors have given approval to the final version of the manuscript.

ABBREVIATIONS

SECCM, scanning electrochemical cell microscopy; AFM, atomic force microscopy; FEM, finite element method; HAP, calcium hydroxyapatite; QRCE, quasi reference counter electrode; TEM, transmission electron microscopy; SEM, scanning electron microscopy; ppm, parts per million; rms, root mean squared; ANOVA, analysis of variance.

1.   A. Dokoumetzidis and P. Macheras, *Int. J. Pharm.*, 2006, **321**, 1-11.
2.   J. C. Orr, V. J. Fabry, O. Aumont, L. Bopp, S. C. Doney, R. A. Feely, A. Gnanadesikan, N. Gruber, A. Ishida, F. Joos, R. M. Key, K. Lindsay, E. Maier-Reimer, R. Matear, P. Monfray, A. Mouchet, R. G. Najjar, G. K. Plattner, K. B. Rodgers, C. L. Sabine, J. L. Sarmiento, R. Schlitzer, R. D. Slater, I. J. Totterdell, M. F. Weirig, Y. Yamanaka and A. Yool, *Nature*, 2005, **437**, 681-686.

3.   R. B. Bjorklund and H. Arwin, *Langmuir*, 1992, **8**, 1709-1714.
4.   E.-S. M. Sherif, R. M. Erasmus and J. D. Comins, *J. Colloid Interface Sci.*, 2007, **309**, 470-477.
5.   D. C. Smith, M. Simon, A. L. Alldredge and F. Azam, *Nature*, 1992, **359**, 139-142.
6.   S. Azarmi, W. Roa and R. Lobenberg, *Int. J. Pharm.*, 2007, **328**, 12-21.
7.   K. D. Demadis, P. Lykoudis, R. G. Raptis and G. Mezei, *Cryst. Growth Des.*, 2006, **6**, 1064-1067.
8.   J. Desarnaud, O. Grauby, P. Bromblet, J.-M. Vallet and A. Baronnett, *Cryst. Growth Des.*, 2013, **13**, 1067-1074.
9.   J. Kameda, H. Sugimori and T. Murakami, *Phys. Chem. Miner.*, 2009, **36**, 537-544.
10.   T. C. Mauldin and M. R. Kessler, *J. Mater. Chem.*, 2010, **20**, 4198-4206.
11.   M. Peruffo, M. M. Mbogoro, M. A. Edwards and P. R. Unwin, *Phys. Chem. Chem. Phys.*, 2013, **15**, 1956-1965.
12.   H.-D. Yu, D. Yang, D. Wang and M.-Y. Han, *Adv. Mater.*, 2010, **22**, 3181-3184.
13.   P. R. Unwin and J. V. Macpherson, *Chem. Soc. Rev.*, 1995, **24**, 109-119.
14.   P. R. Unwin, *J. Chem. Soc., Faraday Trans.*, 1998, **94**, 3183-3195.
15.   C. Robinson, R. C. Shore, S. J. Brookes, S. Strafford, S. R. Wood and J. Kirkham, *Crit. Rev. Oral Biol. Medicine*, 2000, **11**, 481-495.
16.   A. Boyde, in *Teeth*, Springer Berlin Heidelberg, 1989, vol. 5 / 6, pp. 309-473.
17.   R. P. Shellis, *Arch. Oral Biol.*, 1984, **29**, 697-705.
18.   M. I. Kay, R. A. Young and A. S. Posner, *Nature*, 1964, **204**, 1050-1052.
19.   L. F. Francisconi, H. M. Honorio, D. Rios, A. C. Magalhaes, M. A. A. M. Machado and M. A. R. Buzalaf, *Oper. Dent.*, 2008, **33**, 203-208.
20.   N. X. West, J. A. Hughes and M. Addy, *J. Oral Rehabil.*, 2000, **27**, 875-880.
21.   W. I. Higuchi, J. A. Gray, J. J. Hefferren and P. R. Patel, *J. Dent. Res.*, 1965, **44**, 330-341.
22.   R. W. Phillips and G. Van Huysen, *J. Chem. Educ.*, 1946, **23**, 579.
23.   J. A. Gray, *J. Dent. Res.*, 1962, **41**, 633-645.
24.   K.-Y. Kwon, E. Wang, A. Chung, N. Chang and S.-W. Lee, *J. Phys. Chem. C*, 2009, **113**, 3369-3372.
25.   K. G. Scheckel and J. A. Ryan, *Environ. Sci. Technol.*, 2002, **36**, 2198-2204.
26.   S. V. Dorozhkin, *Prog. Cryst. Growth Charact. Mater.*, 2002, **44**, 45-61.
27.   H. G. Linge and G. H. Nancolla, *Calcif. Tissue Res.*, 1973, **12**, 193-208.
28.   M.-S. Wu, W. I. Higuchi, J. L. Fox and M. Friedman, *J. Dent. Res.*, 1976, **55**, 496-505.
29.   D. W. Bishop, J. D. Eick, G. H. Nancolla and W. D. White, *J. Dent. Res.*, 1974, **53**, 198-198.
30.   W. D. White and G. H. Nancollas, *J. Dent. Res.*, 1980, **59**, 1180-1186.
31.   M. S. Wu, W. I. Higuchi, J. L. Fox and M. Friedman, *J. Dent. Res.*, 1976, **55**, 496-505.
32.   W. White and G. H. Nancollas, *J. Dent. Res.*, 1977, **56**, 524-530.
33.   G. H. Nancollas, K. Sawada and E. Schuttringer, in *Biomineralization and Biological Metal Accumulation*, eds. P. Westbroek and E. W. de Jong, Springer Netherlands, 1983, pp. 155-169.
34.   J. C. Voegel and R. M. Frank, *Calcif. Tissue Res.*, 1977, **24**, 19-27.
35.   M. E. Barbour, D. M. Parker, G. C. Allen and K. D. Jandt, *Eur. J. Oral Sci.*, 2003, **111**, 258-262.
36.   M. Finke, K. D. Jandt and D. M. Parker, *J. Colloid Interface Sci.*, 2000, **232**, 156-164.
37.   A. Pyne, W. Marks, L. M. Picco, P. G. Dunton, A. Ulcinas, M. E. Barbour, S. B. Jones, J. Gimzewski and M. J. Miles, *Arch. Histol. Cytol.*, 2009, **72**, 209-215.
38.   N. W. Johnson, D. F. G. Poole and J. E. Tyler, *Arch. Oral Biol.*, 1971, **16**, 385-394.
39.   L. J. Wang, R. K. Tang, T. Bonstein, C. A. Orme, P. J. Bush and G. H. Nancollas, *J. Phys. Chem. B*, 2005, **109**, 999-1005.
40.   C.-A. McGeouch, M. A. Edwards, M. M. Mbogoro, C. Parkinson and P. R. Unwin, *Anal. Chem.*, 2010, **82**, 9322-9328.
41.   L. Qin, W. Zhang, J. Lu, A. G. Stack and L. Wang, *Environ. Sci. Technol.*, 2013, **47**, 13365-13374.
42.   Q. Y. Ma, T. J. Logan, S. J. Traina and J. A. Ryan, *Environ. Sci. Technol.*, 1994, **28**, 408-418.
43.   Y. Tanizawa, K. Sawamura and T. Suzuki, *J. Chem. Soc., Faraday Trans.*, 1990, **86**, 1071-1075.
44.   R. D. Martin, M. A. Beeston, P. R. Unwin and M. E. Laing, *J. Chem. Soc., Faraday Trans.*, 1994, **90**, 3109-3115.
45.   H. G. McCann, *Arch. Oral Biol.*, 1968, **13**, 987-1001.
46.   J. M. Ten Cate and J. D. B. Featherstone, *Crit. Rev. Oral Biol. Med.*, 1991, **2**, 283-296.
47.   M. Peld, K. Tõnsuaadu and V. Bender, *Environ. Sci. Technol.*, 2004, **38**, 5626-5631.
48.   J. A. Gray, *J. Dent. Res.*, 1965, **44**, 493-501.
49.   K.-Y. Kwon, E. Wang, M. Nofal and S.-W. Lee, *Langmuir*, 2011, **27**, 5335-5339.
50.   X. Wang, A. Klocke, B. Mihailova, L. Tosheva and U. Bismayer, *J. Phys. Chem. B*, 2008, **112**, 8840-8848.
51.   S. Loher, W. J. Stark, M. Maciejewski, A. Baiker, S. E. Pratsinis, D. Reichardt, F. Maspero, F. Krumeich and D. Günther, *Chem. Mater.*, 2005, **17**, 36-42.
52.   Y. Honda, T. Anada, S. Morimoto, Y. Shiwaku and O. Suzuki, *Cryst. Growth Des.*, 2011, **11**, 1462-1468.
53.   K. O. A. Chin and G. H. Nancollas, *Langmuir*, 1991, **7**, 2175-2179.
54.   N. R. Mohammed, M. Mneimne, R. G. Hill, M. Al-Jawad, R. J. M. Lynch and P. Anderson, *J. Dent.*, 2014, **42**, 1096-1104.
55.   N. Ebejer, M. Schnippering, A. W. Colburn, M. A. Edwards and P. R. Unwin, *Anal. Chem.*, 2010, **82**, 9141-9145.
56.   M. E. Snowden, A. G. Guell, S. C. S. Lai, K. McKelvey, N. Ebejer, M. A. O'Connell, A. W. Colburn and P. R. Unwin, *Anal. Chem.*, 2012, **84**, 2483-2491.
57.   K. McKelvey, M. A. O'Connell and P. R. Unwin, *Chem. Commun.*, 2013, **49**, 2986-2988.
58.   N. Ebejer, A. G. Guell, S. C. S. Lai, K. McKelvey, M. E. Snowden and P. R. Unwin, *Annu. Rev. Anal. Chem. (Palo Alto Calif.)*, 2013, **6**, 329-351.
59.   S. L. Kinnear, K. McKelvey, M. E. Snowden, M. Peruffo, A. W. Colburn and P. R. Unwin, *Langmuir*, 2013, **29**, 15565-15572.

60.   A. S. Parker, A. N. Patel, R. Al Botros, M. E. Snowden, K. McKelvey, P. R. Unwin, A. T. Ashcroft, M. Carvell, A. Joiner and M. Peruffo, *J. Dent.*, 2014, **Supplement 1, 42**, S21-S29.
61.   C.-H. Chen, K. E. Meadows, A. Cuharuc, S. C. S. Lai and P. R. Unwin, *Phys. Chem. Chem. Phys.*, 2014, **16**, 18545-18552.
62.   D. R. Lide, *CRC Handbook of Chemistry and Physics, 90th Edition*, Taylor & Francis, 2009.
63.   P. W. Brown and B. Constantz, *Hydroxyapatite and Related Materials*, CRC Press, 1994.